4-2016

Liana canopy cover mapped throughout a tropical forest with high-fidelity imaging spectroscopy

David C. Marvin
Carnegie Institution for Science

Gregory P. Asner
Carnegie Institution for Science

Stefan A. Schnitzer
Marquette University, stefan.schnitzer@marquette.edu

Biology Faculty Research and Publications/College of Arts and Sciences

Liana canopy cover mapped throughout a tropical forest with high-fidelity imaging spectroscopy

David C. Marvin
Department of Global Ecology, Carnegie Institution for Science, 260 Panama St., Stanford, CA 94305, USA
Department of Ecology and Evolutionary Biology, University of Michigan, 830 N. University Ave., Ann Arbor, MI

Gregory P. Asner
Department of Global Ecology, Carnegie Institution for Science, 260 Panama St., Stanford, CA

Stefan A. Schnitzer
Department of Biological Sciences, Marquette University, P.O. Box 1881, Milwaukee, WI
Smithsonian Tropical Research Institute, Apartado Postal 0843-03092, Panama

Abstract

Increasing size and abundance of lianas relative to trees are pervasive changes in Neotropical forests that may lead to reduced forest carbon stocks. Yet the liana growth form is chronically understudied in large-scale tropical forest censuses, resulting in few data on the scale, cause, and impact of increasing lianas. Satellite and airborne remote sensing provide potential tools to map and monitor lianas at much larger spatial and rapid

temporal scales than are possible with plot-based forest censuses. We combined high-resolution airborne imaging spectroscopy and a ground-based tree canopy census to investigate whether tree canopies supporting lianas could be discriminated from tree canopies with no liana coverage. Using support vector machine algorithms, we achieved accuracies of nearly 90% in discriminating the presence–absence of lianas, and low error (15.7% RMSE) when predicting liana percent canopy cover. When applied to the full image of the study site, our model had a 4.1% false-positive error rate as validated against an independent plot-level dataset of liana canopy cover. Using the derived liana cover classification map, we show that 6.1%–10.2% of the 1823 ha study site has high-to-severe (50–100%) liana canopy cover. Given that levels of liana infestation are increasing in Neotropical forests and can result in high tree mortality, the extent of high-to-severe liana canopy cover across the landscape may have broad implications for ecosystem function and forest carbon storage. The ability to accurately map landscape-scale liana infestation is crucial to quantifying their effects on forest function and uncovering the mechanisms underlying their increase.

1. Introduction

Tropical forests are a critical part of the global climate system and carbon cycle. Intact tropical forests alone store c. 1.19 ± 0.41 Pg carbon yr^{-1} from the atmosphere (Pan et al., 2011), an amount equivalent to 12.1% of total global carbon emissions in 2013 (Le Quere et al., 2014). For perspective, this amount of carbon is greater than all yearly carbon emissions from the European Union (CDIAC, 2012). Recently, plot-based studies in the Neotropics have documented pervasive changes in old-growth forests that may alter their role in the global carbon cycle. These changes include increased biomass and productivity (Phillips et al., 2009; but see Brienen et al., 2015), increased tree turnover (Phillips, Baker, Arroyo, & Higuchi, 2004), and shifted floristic composition (e.g., Laurance et al., 2004).

Tropical lianas (woody vines) are reported to be increasing relative to trees in Neotropical forests over recent decades (Schnitzer, S. A. and Bongers, F., 2011, Schnitzer, S. A., et al., 2012, Yorke, S. R., et al., 2013). Reported annual increases in liana stem density range from 0.23% to 7.8%, while in the study areas trees either underwent smaller annual increases or have declined in stem abundance (Chave, J., et al., 2008, Phillips, O. L., et al., 2002, Schnitzer, S. A., et al., 2012, Yorke, S. R., et al., 2013). These same studies found increases in liana basal area rangingfrom 0.3% to 4.6% annually over the same time period, with just a 0.34% per year increase in tree basal area. Liana seedling recruitment, reproduction, leaf litter production, and canopy cover have also increased relative to trees (Benítez-Malvido, J. and Martinez-Ramos, M., 2003, Ingwell, L. L., et al., 2010, Wright, S. J., et al., 2004).

The reported relative increase of lianas has broad implications for tropical forests and the global carbon cycle. Lianas commonly comprise a large proportion of the woody species and stem numbers in tropical forests (Schnitzer et al., 2012); however, lianas constitute only a small proportion of total tropical forest biomass (e.g., DeWalt & Chave, 2004). Nevertheless, lianas have a disproportionately large negative effect on tree biomass accumulation (van der Heijden, Powers, & Schnitzer, 2015) by reducing tree diameter increment (e.g., Schnitzer, van der Heijden, Mascaro, & Carson, 2014), leaf productivity (e.g., Perez-Salicrup, Sork, & Putz, 2001), sap flow velocity (Álvarez-Cansino, Schnitzer, Reid, & Powers, 2015), and stem height (Perez-Salicrup, 2001). Lianas also decrease forest carbon accumulation and long-term storage through reduced tree fecundity (e.g., Nabe-Nielsen, Kollmann, & Pena-Claros, 2009), increased tree mortality (e.g., Phillips et al., 2002), and suppressed tree regeneration (e.g., Schnitzer & Carson, 2010). Trees that support large lianas or severe liana infestations have a 40–100% increased mortality risk compared to those with low to no liana infestation (Ingwell, L. L., et al., 2010, Phillips, O. L., et al., 2002). The disproportionately negative effect that lianas can exert on tree growth, reproduction, and lifespan, combined with their low contribution to forest

biomass (Duran & Gianoli, 2013), suggest a future in which Neotropical forests will absorb and store less atmospheric carbon dioxide annually (van der Heijden, Schnitzer, Powers, & Phillips, 2013).

Despite the negative consequences of increasing liana size and abundance, few studies have examined temporal changes in tropical liana abundance and size. While some studies rely on proxy data (i.e., flowering, productivity, recruitment) to establish that lianas are increasing relative to trees, only five studies have used stem or canopy-based censuses (Chave, J., et al., 2008, Ingwell, L. L., et al., 2010, Phillips, O. L., et al., 2002, Schnitzer, S. A., et al., 2012, Yorke, S. R., et al., 2013). These studies examine a total of 160 ha of Neotropical old-growth tropical forests among 150 plots ranging in size from 0.1 ha to 50 ha. The limited spatial extent of long-term liana censuses restricts our ability to assess the scale and impact of increasing tropical lianas.

Satellite and airborne remote sensing may allow ecologists to map and monitor liana abundance at broader spatial scales with higher frequency than is feasible with plot-based censuses. Previous lab and field studies have documented clear differences between liana and tree spectral reflectance signatures, with supporting foliar chemical and structural data (Table S1). These studies document specific regions of the electromagnetic spectrum where lianas and trees are separable, and show that leaf-level differences scale up to the canopy level. Only one study has successfully used remote sensing to map liana abundance at the landscape-scale. This study successfully identified 1150 ha of forest with severe liana canopy cover using moderate-resolution (15–30 m) hyperspectral and multispectral imagery (Foster, Townsend, & Zganjar, 2008). However, the liana patches mapped in this study were within large (> 0.45 ha) forest gaps with severe (c. > 80%) liana cover, making it unlikely the same moderate-resolution imagery approach could successfully map liana abundance and distribution in contiguous closed-canopy forest where liana cover is far more variable and less concentrated. Other studies have attempted liana and tree discrimination at the leaf level (Castro-Esau, K., et al., 2004, Hesketh, M. and Sánchez-Azofeifa, G. A., 2012) and canopy level (Kalacska, Bohlman, Sánchez-Azofeifa, Castro-Esau, & Caelli, 2007), but did not develop methods appropriate for mapping lianas at landscape-scales.

Recent advances in high-resolution imaging spectroscopy and analysis now provide the potential to distinguish lianas from trees at the sub-canopy scale. High spatial and spectral resolution imaging spectrometers are able to discriminate subtle differences in leaf chemistry and structure (Asner, G. P. and Martin, R. E., 2010, Kampe, T. U., et al., 2010), and new applications of machine learning algorithms have proven accurate for discriminating individual tree species (Baldeck, C. A., et al., 2015, Féret, J.-B. and Asner, G. P., 2012).

Our goal was to map the distribution and abundance of lianas throughout a well-studied Neotropical forest using high-resolution imaging spectroscopy, and examine associations between liana canopy cover and the local topography or forest structure. Using imagery collected over central Panama by the Carnegie Airborne Observatory, combined with a ground-based liana canopy census of nearly 800 trees, we asked whether liana canopy cover could be mapped over 1823 ha of contiguous closed-canopy Neotropical forest. We employed machine learning classification and regression algorithms, and evaluated their ability to detect liana presence–absence and predict the percent canopy cover of lianas.

2. Methods

2.1. Site

The study site is a mainland peninsula of the Barro Colorado Nature Monument in the Republic of Panama (Fig. 1). The Gigante Peninsula (9.1°N, 79.8°W) is covered by a seasonally-dry, secondary tropical moist forest > 200 years old, interspersed with 50–70 year old forest patches recovering from agricultural disturbance (D. Dent, unpublished data). On nearby Barro Colorado Island 28% of canopy tree species are dry-season deciduous but only result in a deciduous fractional crown area of ~ 10% (Richard Condit et al., 2000), with only 3 of the 165 liana species known to be dry-season deciduous (Putz, F. E. and Windsor, D. M., 1987, Schnitzer, S. A., et al.,

2012). An assessment of regional deciduousness using satellite imagery found that the Gigante Peninsula was about 8–9% deciduous by area (Bohlman, 2010). The geological substrate is a Miocene basalt (R. H. Stewart, Stewart, & Woodring, 1980), and the soils are considered relatively fertile for the lowland tropics (Wright et al., 2011). On nearby Barro Colorado Island, monthly precipitation averages c. 290 mm in the wet season (May–December) and c. 70 mm in the dry season (January–April) (STRI, 2013).
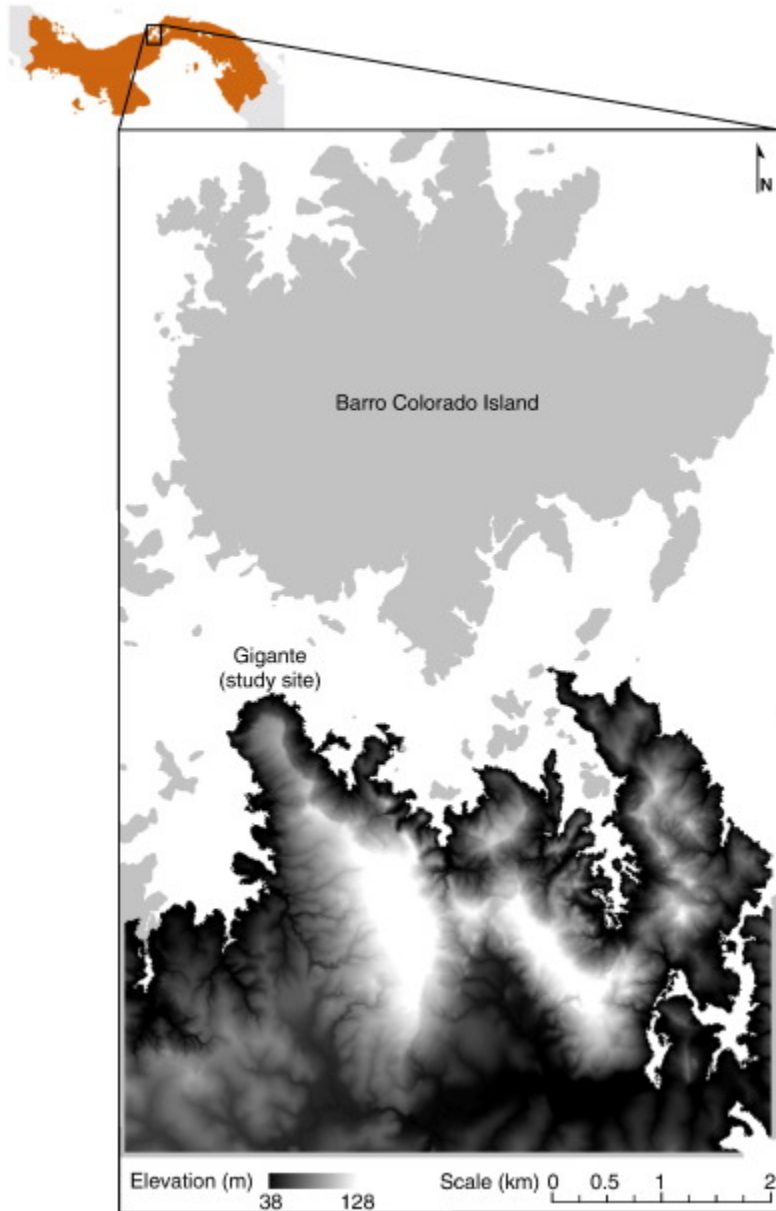

Fig. 1. Gigante Peninsula study site in central Panama. A LiDAR-derived digital elevation model (DEM) is displayed over the extent of the study site.

2.2. Imagery

In the dry season of February of 2012, the Carnegie Airborne Observatory (CAO) Airborne Taxonomic Mapping System (AToMS) acquired high-resolution data of the site with an integrated (i) full-spectral range (visible-to-shortwave infrared) imaging spectrometer, (ii) a visible-to-near infrared (VNIR) imaging spectrometer, and (iii) a full-waveform light detection and ranging (LiDAR) (Asner et al., 2012). The AToMS visible-to-shortwave infrared imaging spectrometer (VSWIR) measures spectral radiance in 481 contiguous channels spanning the 252–

2648 nm wavelength range. At a 2000 m [flight altitude](), the VSWIR data collection provided 2.0 m ground sampling distance, or pixel size, throughout each study landscape. The VNIR imaging spectrometer collects 288 contiguous [spectral bands]() over a smaller range (365–1052 nm) than the VSWIR, but at twice the [spatial resolution]() (1.0 m at 2000 m altitude). The AToMS LiDAR is a dual [laser, scanning](), [waveform]()system capable of operating at 500,000 laser shots per second. Because the airborne data were collected along adjacent flightlines with 50% overlap, the LiDAR point density was 2 shots m^{-2}, or 8 shots per VSWIR pixel. This level of over-sampling ensured that the derived LiDAR measurements were highly precise in horizontal and vertical space ([Asner et al., 2012]()).

The LiDAR data were used to precisely orthorectify and geolocate the VSWIR data and to provide a means to mask [canopy gaps]() and shadows, water and exposed soil in the spectral data. We used the LiDAR point cloud to interpolate a [raster]() [digital terrain model]() (DTM) for the ground surface. A digital surface model (DSM) was similarly created based on [interpolations]() of all first-return points. Measurement of the vertical difference between the [DTM]() and DSM yielded a top-of-canopy height (TCH) model. Treefall gaps were defined based on the difference in relative height from the surrounding canopy (Marvin & Asner, in review). We created a TCH_{mean} layer using a mean smoothing filter with a one ha kernel. The TCH_{mean} was subtracted from the original TCH layer, and divided by TCH_{mean} to produce a relative TCH layer. Treefall gaps were classified as having a relative TCH of − 0.7 to − 1.0, or 70–100% below the mean forest height of the surrounding 1 ha.

The VNIR and VSWIR spectrometer data were radiometrically corrected from raw digital number (DN) values to radiance (W sr^{-1} m^{-2} nm^{-1}) using a flat-field [correction, radiometric]() calibration coefficients and spectral calibration data collected in the laboratory, with further post-processing described in detail by [Asner et al. (2012)](). [Reflectance]() imagery was corrected for cross-track [brightness]() gradients using a [bidirectional reflectance]() [distribution function]() (BRDF) model described by ([Colgan, Baldeck, Féret, & Asner, 2012]()). The reflectance imagery was then orthorectified to the LiDAR DSM.

We used a 2900 by 2200 pixel VSWIR image of the study site covering 1823 ha of the mainland Gigante Peninsula. We calculated the [normalized difference vegetation index]() (NDVI) as (NIR − VIS) / (NIR + VIS) where NIR and VIS are the reflectances at 800 and 680 nm, respectively. We filtered the data to retain only well-lit ([Asner et al., 2007]()), live vegetation pixels with an [NDVI]() ≥ 0.8 and mean [near infrared]() (850–1050 nm) reflectance > 20%. We removed water [absorption bands]() and bands near the instrument measurement boundaries, resulting in a 178-band VSWIR image used for the analyses described below. We used a 4-band subset VNIR image of the same area to georeference individual tree crowns in the field. All [image processing](), data extraction, and layer creation was performed in IDL/ENVI (Exelis, Boulder, CO USA) and/or SAGA GIS ([SAGA GIS, 2014]()).

2.3. Field data

2.3.1. Individual tree crown georeferencing

During July and August 2013, we collected field data outside the boundaries of ongoing forest [manipulation]() experiments at the study site. We used a combined tablet computer (Apple Inc., Cupertino, CA USA) and Bluetooth-enabled GPS/GLONASS receiver (Garmin Ltd., Olathe, KS USA) system to navigate and collect field data within the study site. We uploaded the VNIR image of the study site to the application iGIS (Geometry Pty Ltd., Tasmania, Australia) on the tablet system, allowing us to georeference individual tree crowns directly on the imagery. Once an individual tree crown in the image was confirmed on the ground, we marked the tree in the iGIS application and recorded all data in a custom data entry pop-up form linked to each point. We only marked trees ≥ 10 cm diameter at breast height (dbh, as described by [Condit (1998)]()) that had 90% of the crown fully sun-exposed and were clearly identifiable on the imagery (n = 780). All point coordinates and associated data were exported from the tablet system as shapefiles.

2.3.2. Liana canopy cover survey

We assessed the percent cover of lianas in each georeferenced tree canopy using a modified version of the crown occupation index (cf. Clark, D. B. and Clark, D. A., 1990, van der Heijden, G. M. F., et al., 2010), as follows. The field team consisted of four people working in pairs, which rotated membership each day. In our version of the index, the centroid of each tree's canopy was first determined, and the crown then visually bisected with north-south and east-west lines, forming four quadrants. Independent of their partner, each person thoroughly (spending up to 20 min per crown) assessed each quadrant for the percent cover of lianas to the nearest 5%. The two partners then discussed the quadrant estimates and mutually agreed on a final estimate for each. To assess reliability among the field team, one tree was independently assessed by each of the four members at the beginning of each field day before splitting into pairs. We also measured the dbh and of each tree and noted any major crown gaps or irregularities. We supplemented this dataset with 11 tree crowns from field survey plots from a nearby experimental liana study (see below for details).

2.3.3. Individual tree crown pixel extraction

Using the VNIR image in ERDAS IMAGINE (Hexagon Intergraph, Madison, AL USA) or ENVI software, we manually outlined the sunlit portions of the crown for each georeferenced tree, carefully avoiding shaded areas and crown edges. We extracted pixels from the VSWIR image using the crown polygons that encompassed at least three image pixels (smaller crowns were excluded due to difficulty of confidently finding their locations on the imagery in the field). This yielded a total of 554 usable tree crowns in the analysis, representing a total of 21,620 pixels. The distributions of individual tree crown liana canopy cover and associated number of VSWIR imagery pixels are presented in Fig. 2.
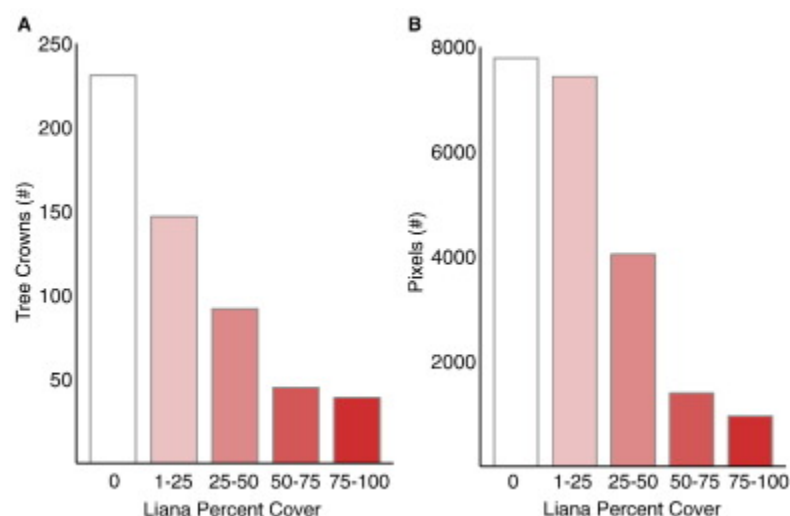

Fig. 2. (A) Distribution of individual tree crowns at the central Panama study site by level of liana canopy cover as determined by our field survey of tree crowns. (B) Distribution of VSWIR imagery pixels derived from geolocated liana canopy cover survey of tree crowns.

2.4. Support vector machine classification

Support vector machine (SVM) classification is a supervised machine learning technique that is increasingly being used by the remote sensing community (Mountrakis, Im, & Ogole, 2011). We chose to use SVM because produces comparable or better results than other algorithms such as discriminant analysis, maximum likelihood, or artificial neural networks (Mountrakis et al., 2011). SVM is a non-parametric classifier that makes no assumptions about the underlying distribution of the data, and thus SVM is particularly useful in remote sensing applications where the distributions of imagery data are often unknown. SVM projects samples of different classes into multidimensional space and fits a hyperplane that best defines the boundaries separating the

classes. To [transform](#) the hyperspectral data into higher dimensional space, we used the radial basis function (RBF) kernel because it has a low number of input parameters and higher performance relative to other [kernel functions](#) ([Féret & Asner, 2012](#)). Other advantages of SVM are the ability to efficiently process large input spaces and its insensitivity to the Hughes phenomenon, or the decrease in classification accuracy after passing a threshold number of input features ([Melgani & Bruzzone, 2004](#)). Thus SVM allows full use of the high dimensionality of hyperspectral data with relatively few training samples ([Gualtieri & Cromp, 1999](#)). All data processing and analysis was performed in the open-source statistical software program R ([R Development Core Team, 2014](#)). SVM implementation was performed using the R package 'e1071' ([Meyer, 2012](#)).

2.5. SVM optimization, validation, and visualization

We performed a two-step SVM procedure: first using SVM-classification to produce a binary model of liana presence–absence, followed by SVM-regression to produce a continuous model of liana percent cover trained by only those pixels identified from the binary model as having liana presence. Both model types were tuned using 10-fold cross validation over a reasonable (to constrain computation time and avoid overfitting) set of parameter values to find the optimal set. The parameters to be optimized for the RBF kernel are a) gamma (γ) controlling the flexibility of the classifier — or the [trade-off](#) between model over-fitting and under-fitting ([Ben-Hur & Weston, 2009](#)), and b) penalty or cost (C), controlling the trade-off between model complexity and training errors ([Cortes & Vapnik, 1995](#)). The parameter optimization was performed using a grid search over the values $\gamma = \{e^{-8}, e^{-7}, ..., e^{-2}\}$ and $C = \{e^2, e^3, ..., e^8\}$.

A full binary SVM model (no cross validation) was fit using the optimal set of parameter values as determined by the highest F-score and area under the ROC (receiver operator characteristic) curve from the 10-fold cross validation tuning. The F-score is calculated by F = 2pr / (p + r), where r is the sensitivity or true positive rate and p is the precision, and is intended to yield high but balanced values of the sensitivity and precision of the model. The ROC curve from the cross-validation binary model was used to find the optimal cutoff probability that maximized the true positive rate (0.89) and minimized the false positive rate (0.12) for class separation. We used this cutoff value (0.634) to create a binary mask of only liana-present pixels. Due to insufficient data to train independent binary and regression models, we introduced noise into the binary mask proportional to the error produced by the binary model as follows. We randomly selected pixels from each class of the binary mask and changed them to the opposite class according to the false positive (0.12) and false negative (0.11) rates. We created five binary randomized error masks using this procedure, in order to assess the variance caused by the additional error.

These masks were used as inputs to tune the SVM-regression model for each parameter set in the grid search using 10-fold cross validation. We used the RMSE and R^2 averaged over the five masks to chose the optimal parameter set for creation of a final (no cross validation) full SVM regression model. This final full SVM-regression model was used to predict the canopy cover of lianas over the entire study landscape (see *Landscape Liana Cover Mapping*). Out-of-range values (< 1% and > 100%) predicted by the SVM-regression model were set to 1 and 100, respectively.

The kernel transformation employed by SVM means that direct interpretation of the final model in relation to the input variables (reflectance for each spectral band) is difficult ([Üstün, Melssen, & Buydens, 2007](#)), often leading to [characterizations](#) of SVM or other machine learning algorithms as "black-box" techniques. We used the methods proposed by [Üstün et al. (2007)](#) to determine which wavelengths are most important to the regression results. We obtain feature weights by calculating the inner-product between the final SVM model coefficients (i.e., the support vector weights) and the standardized support vector spectra from the SVM model. We use the standardized support vector spectra rather than the original support vector spectra (as in [Üstün et](#)

al., 2007) because the magnitude of feature weights are suppressed in regions of the spectrum with relatively low reflectance.

2.6. Landscape liana cover mapping

We applied the full binary SVM model to the entire VSWIR imagery to identify those pixels predicted to contain lianas. Liana-containing pixels were then used as inputs into the full SVM-regression model to create a map of predicted liana percent cover on a continuous scale. We removed all isolated groups of less than three liana-containing pixels since this was the minimum tree crown size that was assessed in the field.

For better visualization and comparison to other studies, we binned each pixel into one of four percent liana cover categories: [0–25), [25,50), [50–75), [75–100), and assessed the total liana coverage of the study site from this classified image. Binning should increase user confidence because we cannot quantitatively measure and propagate all sources of uncertainty (e.g., field census, spectral, SVM model) into the final map. We applied a 5 m inland buffer around water features to remove any influence of below-canopy water reflectance. We summed the pixels in each class over the whole image to calculate the landscape-level percent cover of each class.

To validate the full landscape liana cover map, we used data from an ongoing liana removal experiment at the study site (Martinez-Izquierdo, L., et al., in press, van der Heijden, G. M. F., et al., 2015). Eight 80 by 80 m plots had all lianas removed in 2011 and are maintained as liana-free. We calculated the number of pixels incorrectly classified by the SVM as containing lianas in the removal plots to get a landscape-level false positive rate. Eight other plots are unmanipulated controls, and a similar liana canopy cover assessment as described above was conducted annually.

2.7. Topographic and forest structure analysis

We assessed whether liana cover was associated with variables related to the underlying topography or forest structure. To match the pixel dimensions of the VSWIR image and resulting classification, we resampled the LiDAR-derived DEM to a 2 m pixel size. Elevation data was extracted directly from the DEM. Using the 'topographic modeling' feature in ENVI, we used the DEM to create slope and aspect models at this same spatial resolution. The LiDAR top-of-canopy-height (TCH) and canopy gap layers (see Imagery) were both resampled to a 2 m pixel size. A canopy gap proximity layer was created using a Euclidean distance transform with the gap layer as the source. Each layer (elevation, slope, aspect, TCH, and gap proximity) was used separately as a predictor in a linear regression model with liana cover as the response.

3. Results

3.1. SVM performance

The optimal binary SVM model (presence–absence) from the 10-fold cross validation tuning yielded an F-score of 0.91 and specificity of 0.81, with an area under the ROC curve of 0.94 (Fig. S1, Table S2). The optimal SVM-regression model from the 10-fold cross validation tuning yielded an average (over the five masks) RMSE of 15.65 (0.05 sd) and R^2 of 0.59 (0.003 sd). The low variation among the results of the five randomized error masks indicates the SVM-regression signal is not affected by the binary SVM model prediction error. A scatterplot of observed and SVM-regression predicted liana percent cover (Fig. S2) shows a reasonable linear fit, with overestimation of liana cover below 25% and underestimation of liana cover occurring from 25–100%.

While the spectra used to train SVM models show substantial overlap in all regions of the spectrum (Fig. 3A, B), the SVM feature weights (i.e., from (Üstün et al., 2007)) uncover the importance of each commonly defined spectral regions to the final SVM classification (Fig. 3C). Multiple wavelengths in each region had large feature weights, signifying their relevance to classifying liana canopy cover. The visible region (400–690 nm) clearly had

the highest average feature weight, followed by the near infrared (NIR, 700–1340 nm) and the shortwave infrared-1 (SWIR-1, 1420–1790 nm) regions (Fig. 3C). The SWIR-2 (2010–2460 nm) region had the lowest average feature weights (70% lower than the visible) but is still important to the SVM classification.
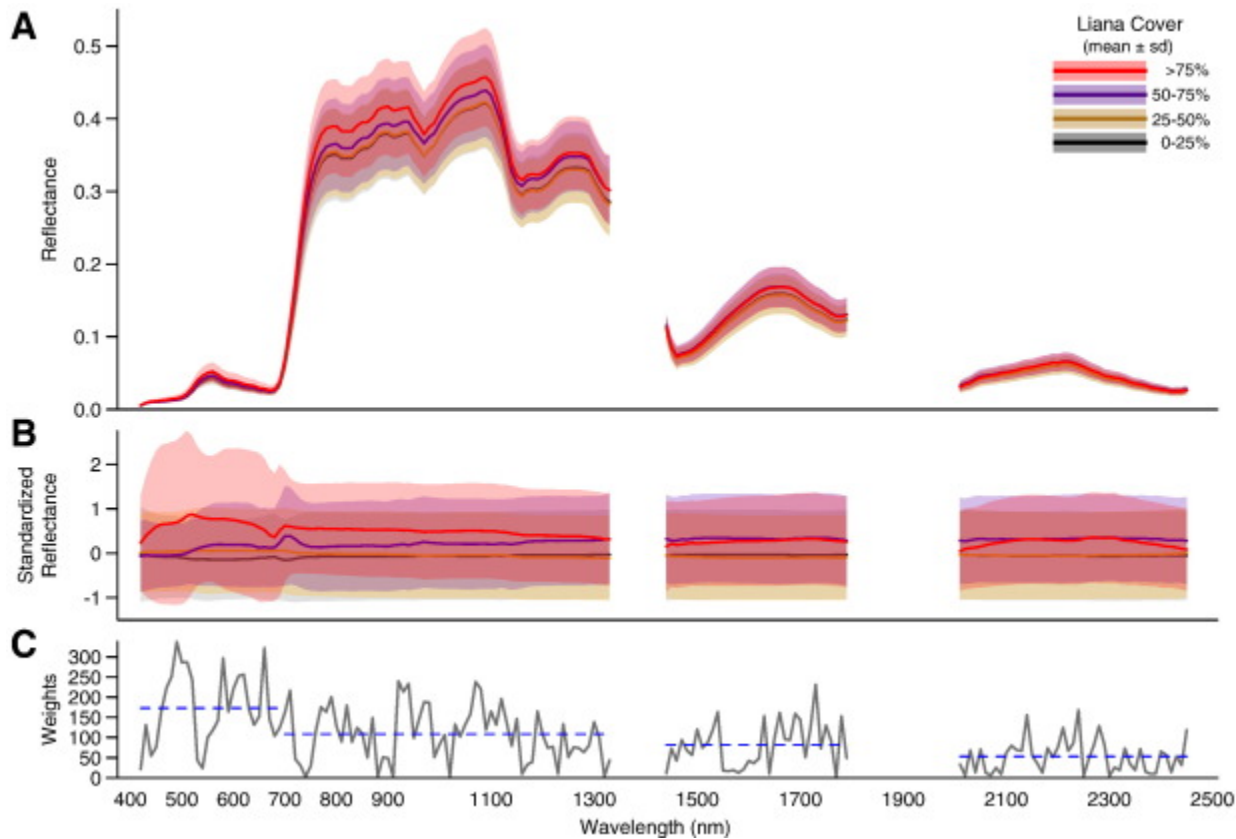

Fig. 3. Spectra used to train the optimal severe liana cover SVM model are presented as (A) unstandardized and (B) standardized ($\mu = 0$, $\sigma = 1$) reflectance values. Lines are mean reflectance for training spectra (shading is ± 1 SD). The standardization of reflectance values in (B) removes the signal of reflectance magnitude or "brightness" such that relative differences in regions of the spectrum are more apparent. Importance of each region to the SVM classification is shown in (C) with feature weights in gray with blue dashed lines representing the mean feature weight within each of the four spectral regions (visible, NIR, SWIR-1, SWIR-2).

3.2. Landscape liana cover mapping

Applying the binary SVM to the full VSWIR image, we found liana present pixels covered 58.1% of the 1823 ha study site. The SVM-regression model predicted severe (75–100%) and high (50–75%) liana cover over 1.2% and 9.0% of the site, respectively (Fig 4, Fig. S5). Moderate (25–50%) and low (1–25%) liana cover was predicted over 27.0% and 20.9% of the study site, respectively (Figs. S4 and S5). We focus on the severe and high liana cover classifications because they are more relevant to forest ecology (see Discussion), and we are not confident in the low cover class given the RMSE of 15.65%. The combined liana absent and low liana cover classifications totaled 62.8% of the site. These calculations assume that the unclassified pixels (shaded or deciduous, see Methods) of the image (24.2%) have the same distribution of liana cover.
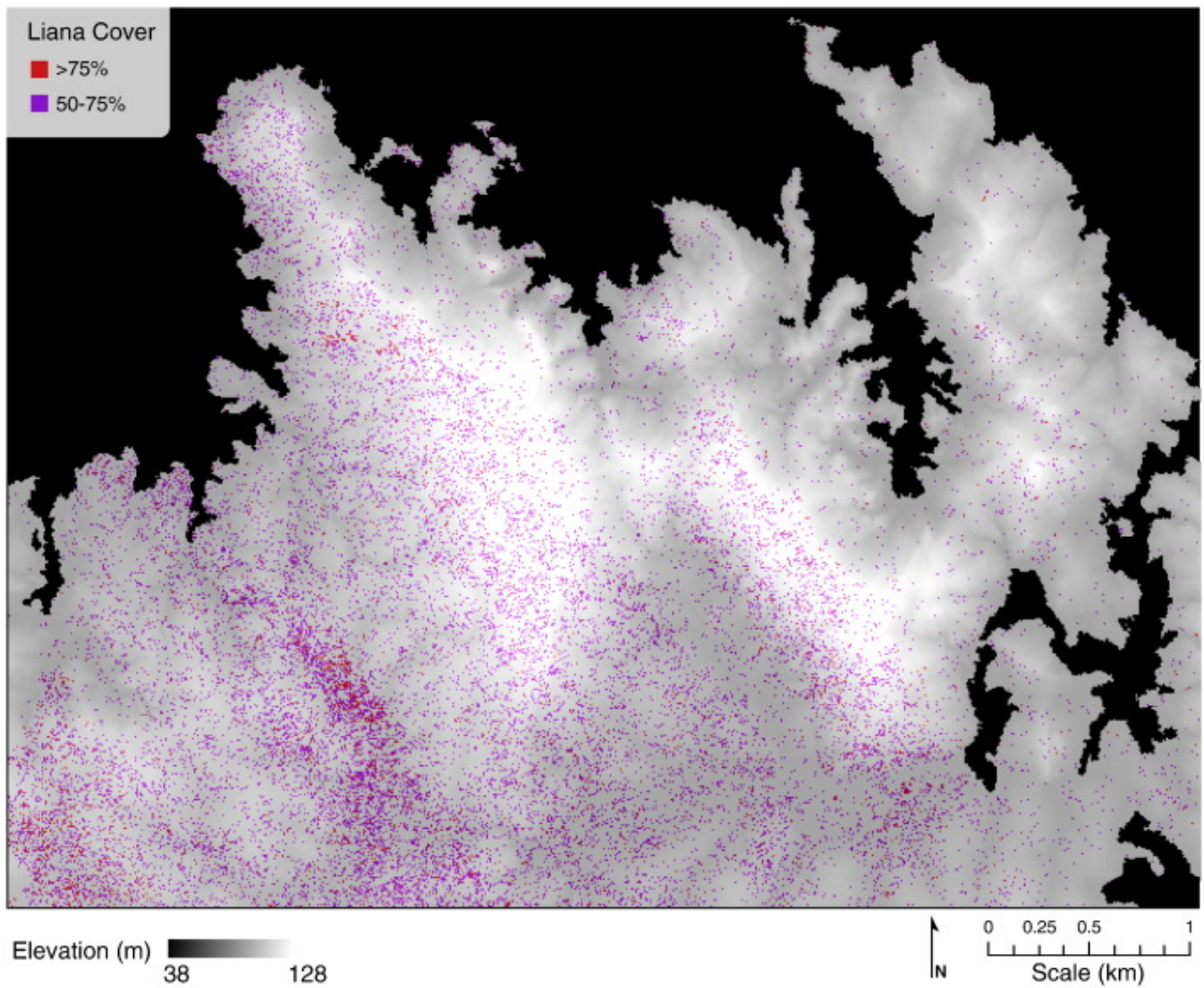
Fig. 4. Landscape liana cover from the SVM-regression model of the full VSWIR image overlaid on top of the DEM for the study site. Continuous liana cover values are binned into high [50–75%) and severe [75–100%) classes for better visualization. See Fig. S4 for a map of the other classes, and Fig. S5 for a map of the continuous range of liana cover.

Examining the classification of the liana experimental removal plots, we found that the SVM-regression model incorrectly classified an average of 4.1 ± 2.0% pixels as containing high-to-severe liana cover per removal plot (i.e., false positives from an area known to contain 0% liana cover). The false positive rates for the moderate and low liana cover classes were 21.5% and 19.5%, respectively. We did not validate the prediction of liana cover in the control plots of the liana removal experiment because we predict liana cover on a per-area basis, while the field estimates are on a per-crown basis. Incorporating the high-to-severe liana cover false positive error rate (4.1%), we estimate a landscape-scale presence of high-to-severe liana cover in the range of 6.1%-10.2%.

3.3. Topographic and forest structure analysis

We found marginal positive associations between liana cover and elevation or aspect (Fig. 5). In both cases less than 1% of the variation in liana cover was explained by elevation or aspect ($R^2_{elevation}$ = 0.004, R^2_{aspect} = 0.002). Additionally, we found marginal negative associations between liana cover and the remaining variables (Fig. 5).

Slope and TCH both explained slightly higher, but still marginal, variation in liana cover (R^2_{slope} = 0.01, R^2_{TCH} = 0.03), while distance to gap explained less than 1% ($R^2_{GapDist}$ = 0.003).
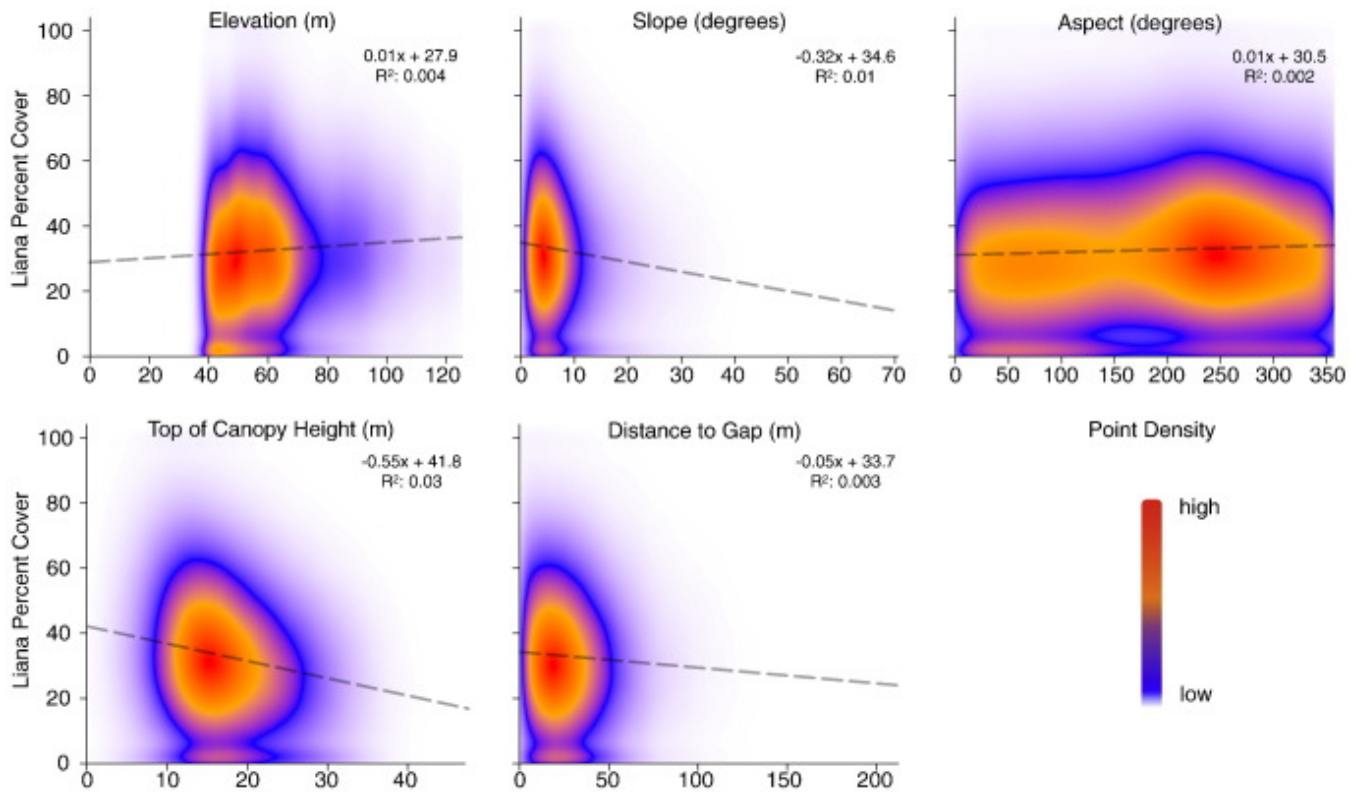

Fig. 5. Associations between mapped continuous liana cover and topographic or forest structural variables (derived from 2 m resolution maps). Dashed line is the fitted linear regression line, with corresponding equation and R^2 value in upper right corner of each panel.

4. Discussion

4.1. Landscape liana distribution

We developed a method to map the distribution of liana canopy coverage at the landscape scale in a contiguous tropical forest. Of the over 1800 ha mapped at the study site, 6.1%–10.2% (111–186 ha) were identified as containing tree canopies with high-to-severe (> 50%) levels of liana cover. Ingwell et al. (2010) reported that 16.0% of the 2127 tree crowns they surveyed on nearby Barro Colorado Island had a liana canopy cover > 75%, and 8.0% of tree crowns had 50–75% liana canopy cover. We find our landscape-scale estimates are consistent with those of three other plot-based estimates from Neotropical sites (van der Heijden et al., 2010) (Fig. 6). The only other landscape-scale study of liana cover identified severe liana canopy cover across 1.5% and 3% of a Bolivian tropical forest (Foster et al., 2008). Thus, we estimate our high-to-severe liana coverage to be generally lower than the range of reported values in other Neotropical forests, at least at the plot-level.
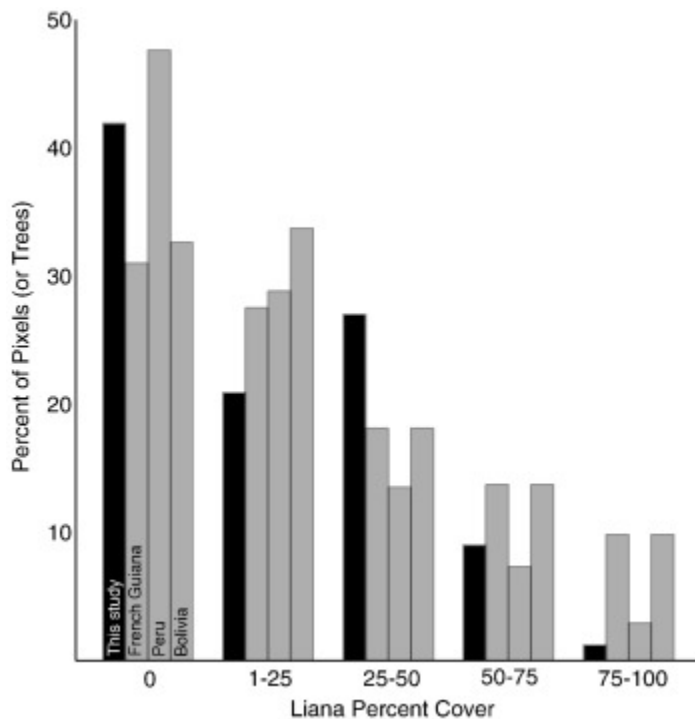
Fig. 6. Distribution of results from the landscape-scale map of this study in percent of pixels (black bars) compared to results from Table 1 in ([van der Heijden et al., 2010](#)) in percent tree crowns (grey bars).

Our 58.1% liana presence from the binary classification matches up well with prior studies that found lianas were present in 53% ([Ingwell et al., 2010](#)), 58% ([van der Heijden & Phillips, 2009](#)), 42% ([Putz, 1983](#)), and 47% ([Putz, 1984](#)) of the trees in Neotropical forests. The presence–absence model applied to the full study site (Fig. S3) produced light diagonal striping resulting from a combination of the mosaicking procedure and/or large cross-track [brightness](#) gradient not corrected by the BRDF model. This striping suggests that low view and/or illumination angle reduces the ability of SVM models to discriminate lianas and trees. If image post-processing is unable to remove these effects, collection of supplemental tree crown training data from affected areas might improve the SVM model predictions.

We did not find strong associations between severe liana cover and topography (slope/elevation/aspect) or forest structure (tree height/canopy gap proximity). Previous studies found that liana stem density is positively associated with treefall gaps (e.g., [Schnitzer & Carson, 2001](#)), higher [soil fertility](#) (but see [Dalling, J. W., et al., 2012](#), [Gentry, A., 1991](#), [Laurance, W., et al., 2001](#)), and flatter terrain ([Dalling et al., 2012](#)). The disparity between our study and previous ones in this area may result from use of liana canopy cover in our analysis, whereas previous studies use liana stem locations. Liana canopies can grow tens of meters horizontally away from their [rooting](#) point ([Penalosa, J., 1984](#), [Putz, F. E., 1984](#)), thereby obscuring potential associations with either topography or forest structure in analyses of liana canopy cover. Another possible explanation for this discrepancy is the spatial grain used for the analyses in each study: the current study used a 2 m spatial grain to assess liana associations with topography and forest structure, whereas previous studies typically use larger spatial grains (≥ 20 m).

The widespread severe liana coverage in tree canopies detected in this study at the plot and landscape scale has major implications for forest carbon dynamics, especially in the context of the reported Neotropical liana size and abundance increase relative to trees ([Schnitzer, S. A. and Bongers, F., 2011](#), [van der Heijden, G. M., et al., 2013](#)). Liana canopy cover is reported to increase significantly as rooted liana [basal area](#) increases in the surrounding 2 m of a tree ([Ingwell et al., 2010](#)). Liana loadings are associated with reductions in the carbon gain

of trees at the stand level by an average of 0.25 Mg C ha^{-1} y^{-1} (van der Heijden & Phillips, 2009), and reduce net annual carbon gain by 76% compared to liana-free forest stands (van der Heijden et al., 2015). While the former study did not estimate the liana canopy coverage of the trees measured, they did find that as the basal area of lianas entering tree canopies increased, the growth rates of those trees strongly decreased (see also Schnitzer & Carson, 2010). In fact, Ingwell et al. (2010) found that the mortality rate of trees with ≥ 75% liana canopy cover was double that of trees supporting no lianas. If high-to-severe liana canopy cover is between 6.1% and 10.2% of this tropical forest landscape, and increasing annually, the impact on forest carbon storage could be substantial. The current and future impact of lianas on forest level carbon dynamics should be represented in global dynamic vegetation models by combining the results from experimental studies of the effect of lianas on forest carbon with remote sensing detection of their distribution and abundance.

4.2. A new approach to liana mapping

Although we focus on high and severe liana canopy cover, we are confident in detecting liana cover as low as 25% (Fig. S4). This level of resolution exceeds the previous liana detection threshold from a study by Kalacska et al. (2007), which found low testing error rates (~ 14%) in discriminating tree crowns with liana coverage > 40% from tree crowns with no lianas. The high accuracy of the presence–absence model was encouraging but further study is needed to verify the lower levels of liana cover (< 25%). Continuing investigation into the lower threshold of liana detection using SVM models will be valuable because even low levels of infestation can affect tree growth (Schnitzer & Carson, 2010).

The success of the SVM approach in distinguishing liana cover from no liana cover can be attributed in part to its use of the entire spectrum in the model. Every region of the spectrum was found to be important to the final model, with the visible region ranking the highest in average feature weight (Fig. 3C). The higher reflectance in the visible region has been previously reported (Table S1), and related to the globally lower area-based leaf chlorophyll content of lianas compared to trees (Asner & Martin, 2012). Most non-machine learning classification methods cannot incorporate the full range of data from imaging spectrometers (often in excess of 100 bands). This loss of relevant information may lead to a reduction in classification accuracy and may have contributed to the lack of successful liana mapping methods to date. Moreover, the very high signal-to-noise ratio of the VSWIR spectrometer increases the likelihood of accurately distinguishing levels of liana cover.

This study was performed on imagery collected from a moist forest during the annual dry season. Previous studies in nearby forests in Panama have shown the differences between the reflectance spectra of lianas and trees are most pronounced in seasonally dry forests (Castro-Esau, K., et al., 2004, Sánchez-Azofeifa, G. A., et al., 2009) and during the dry season (Hesketh & Sánchez-Azofeifa, 2012), but tend to converge in aseasonal forests and during the wet season (Sánchez-Azofeifa et al., 2009). We are not referring to the effect of deciduous species, as deciduous pixels were removed from the model training and predictions using the NDVI and near infrared filtering. Whether the methods presented here would achieve similar detection accuracies during the wet season at this site or in aseasonal forests needs to be explored. However, because liana leaf chemistry differs even in wet forests (Asner & Martin, 2012), our ability to discriminate subtle differences in leaf chemistry using imaging spectroscopy and SVM algorithms may allow differentiation of lianas from trees even in wet forests or during the wet season in seasonal forests.

Several additional factors may affect the accuracy of predicted liana cover in this study. The time lag (15–18 months) between the airborne image acquisition and field data collection allows for unknown increases and/or decreases in liana cover. While this introduces some uncertainty into the final predictions, this relatively short time period should not substantially alter our results. Lianas appear to have faster population dynamics than do trees, but liana turnover occurs over a period of years, not months (Ingwell, L. L., et al., 2010, Phillips, O. L., et al., 2005). Furthermore, annual forest canopy productivity (leaf, flower, fruit, and twig

production) in the control plots of the Gigante liana removal study did not vary from 2011 until 2014 ([van der Heijden et al., 2015](#)) which was the time period of the current study. The extent to which high [species richness](#) (either liana or tree or both) affects our results is unknown, but could introduce additional uncertainty. Many trees, especially those with severe liana cover, have multiple liana species in their crowns, potentially leading to less distinct [spectral reflectance](#)signatures. However, the generalized chemical, physical, and spectral differences between species of lianas and trees presented in Table S1 may mean species richness does not have a large impact on the ability to discriminate lianas and trees using imaging spectroscopy. Expansion of this methodology to additional sites and the collection of species-specific data on tree crown occupation will help to reveal potential sources of uncertainty as this approach matures toward operational status.

By combining ground-based canopy censuses with high-resolution imaging spectroscopy and machine learning algorithms, we have demonstrated the potential of mapping liana abundance at the landscape scale in Neotropical forests — a capacity that we previously lacked. The refinement and deployment of these tools will be critical in verifying, quantifying, and monitoring the increase of lianas relative to trees across the tropics. Moreover, landscape-scale maps will integral in helping to identify the mechanisms underlying increases in liana abundance across the tropics. By uncovering the scale, velocity, and drivers of the liana increase can we truly begin to understand what impact it will have on the role of tropical forests in the global climate system and [carbon cycle](#).

References

Álvarez-Cansino, L., Schnitzer, S. A., Reid, J. P., & Powers, J. S. (2015). Liana competition with tropical trees varies seasonally but not with tree species identity. *Ecology*, *96*(1), 39–45 http://doi.org/10.1890/14-1002.1.

Asner, G. P., & Martin, R. E. (2010). Canopy phylogenetic, chemical and spectral assembly in a lowland Amazonian forest. *New Phytologist, 189*(4), 999–1012 http://doi.org/10.1111/j.1469-8137.2010.03549.x.

Asner, G. P., & Martin, R. E. (2012). Contrasting leaf chemical traits in tropical lianas and trees: Implications for future forest composition. *Ecology Letters, 15*(9), 1001–1007http://doi.org/10.1111/j.1461-0248.2012.01821.x.

Asner, G. P., Knapp, D. E., Boardman, J., Green, R. O., Kennedy-Bowdoin, T., Eastwood, M.,et al. (2012).Carnegie airborne observatory-2: Increasing science data dimensionality via high-fidelity multi-sensor fusion. *Remote Sensing of Environment, 124*, 454–465.

Asner, G. P., Knapp, D. E., Kennedy-Bowdoin, T., Jones, M. O., Martin, R. E., Boardman, J., &Field, C. B. (2007).Carnegie airborne observatory: In-flight fusion of hyperspectral imaging and waveform light

detection and ranging for three-dimensional studies of ecosystems. *Journal of Applied Remote Sensing,1*(1), 013536 http://doi.org/10.1117/1.2794018.

Baldeck, C. A., Asner, G. P., Martin, R. E., Anderson, C. B., Knapp, D. E., Kellner, J. R., &Wright, S. J. (2015). Operational tree species mapping in a diverse tropical forest with airborne imaging spectroscopy. PLoS One, 10(7), e0118403–e0118421 http://doi.org/10.1371/journal.pone.0118403.

Ben-Hur, A., & Weston, J. (2009). A User's Guide to Support Vector Machines. *Methods in Molecular Biology, Vol. 609*. (pp.223–239). Totowa, NJ: Humana Press http://doi.org/10.1007/978-1-60327-241-4_13.

Benítez-Malvido, J., & Martinez-Ramos, M. (2003). Impact of forest fragmentation on understory plant species richness in Amazonia. *Conservation Biology*, 17(2), 389–400.

Bohlman, S. A. (2010). Landscape patterns and environmental controls of deciduousness in forests of central Panama. *Global Ecology and Biogeography*,19(3), 376–385 http://doi.org/10.1111/j.1466-8238.2009.00518.x.

Brienen, R. J. W., Phillips, O. L., Feldpausch, T. R., Gloor, E., Baker, T. R., Lloyd, J., et al. (2015).Long-term decline of the Amazon carbon sink. *Nature, 519*(7543), 344–348http://doi.org/10.1038/nature14283.

Castro-Esau, K., Sánchez-Azofeifa, G. A., & Caelli, T. (2004). Discrimination of lianas and trees with leaf-level hyperspectral data. *Remote Sensing of Environment*, 90(3),353–372 http://doi.org/10.1016/j.rse.2004.01.013.

CDIAC (2012). *Global Carbon Project: Full Global Carbon Budget. U.S. Department of Energy*. (Retrieved from http://cdiac.ornl.gov/).

Chave, J., Olivier, J., Bongers, F., Châtelet, P., Forget, P. -M., Van Der Meer, P., et al. (2008).Above-ground biomass and productivity in a rain forest of eastern South America. *Journal of Tropical Ecology*, 24(04), 355–366 http://doi.org/10.1017/S0266467408005075.

Clark, D. B., & Clark, D. A. (1990). Distribution and effects on tree growth of lianas and woody hemiepiphytes in a Costa Rican tropical wet forest. *Journal of Tropical Ecology*, 6(3), 321–331.

Colgan, M. S., Baldeck, C. A., Féret, J. -B., & Asner, G. P. (2012). Mapping savanna tree species at ecosystem scales using support vector machine classification and BRDF correction on airborne hyperspectral and LiDAR data. *Remote Sensing*, 4, 3462–3480.

Condit, R., Watts, K., Bohlman, S. A., Perez, R., Foster, R. B., & Hubbell, S. P. (2000). Quantifying the deciduousness of tropical forest canopies under varying climates. *Journal of Vegetation Science*, 11(5), 649–658.

Condit, R. (1998). *Tropical Forest Census Plots*, 1–224.

Cortes, C., & Vapnik, V. (1995). Support-vector networks. *Machine Learning*, 20(3),273–297.http://dx.doi.org/10.1007/BF00994018.

Dalling, J. W., Schnitzer, S. A., Baldeck, C., Harms, K. E., John, R., Mangan, S. A., et al. (2012). Resource-based habitat associations in a neotropical liana community. *The Journal of Ecology*, 100(5), 1174–1182.http://dx.doi.org/10.1111/j.1365-2745.2012.01989.x.

DeWalt, S., & Chave, J. (2004). Structure and biomass of four lowland Neotropical forests. *Biotropica,* 36(1), 7–19.

Duran, S. M., & Gianoli, E. (2013). A mechanistic explanation for global patterns of liana abundance and distribution. *Biology Letters*, 166(4), 20130301.http://dx.doi.org/10.1086/431250.

Féret, J. -B., & Asner, G. P. (2012). Tree species discrimination in tropical forests using airborne imaging spectroscopy. *IEEE Transactions on Geoscience and Remote Sensing, 51*(1), 73–84. http://dx.doi.org/10.1109/TGRS.2012.2199323.

Foster, J., Townsend, P., & Zganjar, C. (2008). Spatial and temporal patterns of gap dominance by low-canopy lianas detected using EO-1 Hyperion and Landsat Thematic Mapper. *Remote Sensing of Environment*, 112(5), 2104–2117. http://dx.doi.org/10.1016/j.rse.2007.07.027.

Gentry, A. (1991). The distribution and evolution of climbing plants. *The Biology of Vines* (pp. 3–50). Cambridge: Cambridge University Press.

Gualtieri, J. A., & Cromp, R. F. (1999). Support vector machines for hyperspectral remote sensing classification. In R. J. Mericsko (Ed.), *Presented at the The 27th AIPR Workshop: Advances in computer-assisted recognition, SPIE*. Vol. 3584. (pp. 221–232). http://dx.doi.org/10.1117/12.339824.

Hesketh, M., & Sánchez-Azofeifa, G. A. (2012). The effect of seasonal spectral variation on species classification in the Panamanian tropical forest. *Remote Sensing of Environment, 118*,73–82.http://dx.doi.org/10.1016/j.rse.2011.11.005.

Ingwell, L. L., Wright, S. J., Becklund, K. K., Hubbell, S. P., & Schnitzer, S. A. (2010). The impact of lianas on 10 years of tree growth and mortality on Barro Colorado Island, Panama. *The Journal of Ecology, 98*(4), 879–887.http://dx.doi.org/10.1111/j.1365-2745.2010.01676.x.

Kalacska, M., Bohlman, S., Sánchez-Azofeifa, G. A., Castro-Esau, K., & Caelli, T. (2007). Hyperspectral discrimination of tropical dry forest lianas and trees: Comparative data reduction approaches at the leaf and canopy levels. *Remote Sensing of Environment, 109*(4), 406–415.http://dx.doi.org/10.1016/j.rse.2007.01.012.

Kampe, T. U., Asner, G. P., Green, R. O., Eastwood, M., Johnson, B. R., & Kuester, M. (2010). Advances in airborne remote sensing of ecosystem processes and properties: Toward high-quality measurement on a global scale. In W. Gao, T. J. Jackson, & J. Wang (Eds.), *Presented at the SPIE optical engineering + applications. SPIE, Vol. 7809*. (pp. 78090J).http://dx.doi.org/10.1117/12.859455(–13).

Laurance, W., Oliveira, A., Laurance, S., Condit, R., Nascimento, H., Sanchez-Thorin, A., et al. (2004). Pervasive alteration of tree communities in undisturbed Amazonian forests. *Nature, 428*(6979), 171–175.

Laurance, W., Perez-Salicrup, D.R., Delamonica, P., Fearnside, P., D'Angelo, S., Jerozolinski, A., et al. (2001). Rain forest fragmentation and the structure of Amazonian liana communities. *Ecology, 82*(1), 105–116.

Le Quere, C., Moriarty, R., Andrew, R. M., Peters, G. P., Ciais, P., Friedlingstein, P., et al. (2014). Global carbon budget 2014. *Earth System Science Data Discussions, 7*(2), 521–610http://doi.org/10.5194/essdd-7-521-2014.

Martinez-Izquierdo, L., Muriel-Garcia, M., Powers, J. S., & Schnitzer, S. A. (2016). Lianas suppress seedling growth and survival of 14 tree species in a Panamanian tropical forest. *Ecology* (in press).

Melgani, F., & Bruzzone, L. (2004). Classification of hyperspectral remote sensing images with support vector machines. *IEEE Transactions on Geoscience and Remote Sensing, 42*(8), 1778–1790.http://dx.doi.org/10.1109/TGRS.2004.831865.

Meyer, T. (2012). *Misc functions of the Department of Statistics (e1071). R package version 1.6-1.*

Mountrakis, G., Im, J., & Ogole, C. (2011). Support vector machines in remote sensing: Areview. *ISPRS Journal of Photogrammetry and Remote Sensing, 66*(3), 247–259.http://dx.doi.org/10.1016/j.isprsjprs.2010.11.001.

Nabe-Nielsen, J., Kollmann, J., & Pena-Claros, M. (2009). Effects of liana load, tree diameter and distances between conspecifics on seed production in tropical timber trees. *Forest Ecology and Management, 257*(3), 987–993.http://dx.doi.org/10.1016/j.foreco.2008.10.033.

Pan, Y., Birdsey, R. A., Fang, J., Houghton, R., Kauppi, P. E., Kurz, W. A., et al. (2011). A large and persistent carbon sink in the world's forests. *Science, 333*(6045), 988–993.http://dx.doi.org/10.1126/science.1201609.

Penalosa, J. (1984). Basal branching and vegetative spread in two tropical rain forest lianas. *Biotropica, 16*,1–9.

Perez-Salicrup, D. R. (2001). Effect of liana cutting on tree regeneration in a liana forest in Amazonian Bolivia. *Ecology, 82*(2), 389–396.

Perez-Salicrup, D. R., Sork, V., & Putz, F. E. (2001). Lianas and trees in a liana forest of Amazonian Bolivia. *Biotropica, 33*(1), 34–47.

Phillips, O. L., Aragão, L. E. O. C., Lewis, S. L., Fisher, J. B., Lloyd, J., Lopez-Gonzalez, G., et al. (2009). Drought sensitivity of the Amazon rainforest. *Science, 323*(5919), 1344–1347.http://dx.doi.org/10.1126/science.1164033

Phillips, O. L., Baker, T., Arroyo, L., & Higuchi, N. (2004). Pattern and process in Amazon tree turnover, 1976–2001. *Philosophical Transactions of the Royal Society, B: Biological Sciences, 359*, 381–407.

Phillips, O. L., Martinez, R., Mendoza, A., Baker, T., & Vargas, P. (2005). Large lianas as hyper dynamic elements of the tropical forest canopy. *Ecology, 86*(5), 1250–1258.

Phillips, O. L., Vasquez Martinez, R., Arroyo, L., Baker, T. R., Killeen, T., Lewis, S. L., et al. (2002). Increasing dominance of large lianas in Amazonian forests. *Nature, 418*(6899), 770–774.http://dx.doi.org/10.1038/nature00926.

Putz,F.E.(1984).The natural history of lianas on Barro Colorado Island, Panama. *Ecology, 65*(6), 1713–1724.

Putz, F. E., & Windsor, D. M. (1987). Liana phenology on Barro Colorado Island, Panama. *Biotropica, 19*(4), 334–341.

R Development Core Team (2014). *R: A language and environment for statistical computing*. Vienna, Austria: R Foundation for Statistical Computing (Retrieved from http://www.R-project.org/).

SAGA GIS (2014). *System for automated geoscientific analyses/SAGA User Group Association*. (www.saga-gis.org).

Sánchez-Azofeifa, G. A., Castro, K., Wright, S. J., Gamon, J., Kalacska, M., Rivard, B., et al. (2009). Differences in leaf traits, leaf internal structure, and spectral reflectance between two communities of lianas and trees: Implications for remote sensing in tropical environments. *Remote Sensing of Environment, 113*(10), 2076–2088.http://dx.doi.org/10.1016/j.rse.2009.05.013.

Schnitzer, S. A., & Bongers, F. (2011). Increasing liana abundance and biomass in tropical forests: emerging patterns and putative mechanisms. *Ecology Letters, 14*(4),397–406http://doi.org/10.1111/j.1461-0248.2011.01590.x

Schnitzer, S. A., & Carson, W. (2001). Treefall gaps and the maintenance of species diversity in a tropical forest. *Ecology, 82*(4), 913–919.

Schnitzer, S. A., & Carson, W. (2010). Lianas suppress tree regeneration and diversity in treefall gaps. *Ecology Letters, 13*(7), 849–857.

Schnitzer, S. A., Mangan, S. A., Dalling, J. W., Baldeck, C. A., Hubbell, S. P., Ledo, A., et al. (2012). Liana abundance, diversity, and distribution on Barro Colorado Island, Panama. *PLoS One, 7*(12), e52114 http://doi.org/10.1371/journal.pone.0052114.

Schnitzer, S. A., van der Heijden, G., Mascaro, J., & Carson, W. P. (2014). Lianas in gaps reduce carbon accumulation in a tropical forest. *Ecology, 95*(11), 3008–3017.http://dx.doi.org/10.1890/13-1718.1.

Stewart, R. H., Stewart, J. L., & Woodring, W. P. (1980). Geologic map of the Panama Canal and vicinity, Republic of Panama. *U.S. geological survey miscellaneous investigations series map I-1232*.

STRI (2013). Physical monitoring program.(Retrieved July 25, 2014, from http://biogeodb.stri.si.edu/physical_monitoring/).

Üstün, B., Melssen, W. J., & Buydens, L. M. C. (2007). Visualisation and interpretation of support vector regression models. *Analytica Chimica Acta*, *595*(1-2), 299–309.http://dx.doi.org/10.1016/j.aca.2007.03.023.

van der Heijden, G. M. F., & Phillips, O. L. (2009). Liana infestation impacts tree growth in a lowland tropical moist forest. *Biogeosciences, 6*(10), 2217–2226.

van der Heijden, G. M. F., Feldpausch, T. R., la Fuente Herrero, d., F., van der Velden, N. K., &Phillips, O. L. (2010). Forest ecology and management. *Forest Ecology and Management., 260*(4), 549–555.http://dx.doi.org/10.1016/j.foreco.2010.05.011.

van der Heijden, G. M. F., Powers, J. S., & Schnitzer, S. A. (2015). Lianas reduce carbonic cumulation and storage in tropical forests. *Proceedings of the National Academy of Sciences of the United States of America, 112*(43), 13267–13271.http://dx.doi.org/10.1073/pnas.1504869112.

van der Heijden, G. M., Schnitzer, S. A., Powers, J. S., & Phillips, O. L. (2013). Liana impacts on carbon cycling, storage and sequestration in tropical forests. *Biotropica, 45*(6),682–692http://doi.org/10.1111/btp.12060.

Wright, S. J., Calderon, O., Hernandez, A., & Paton, S. (2004). Are lianas increasing in importance in tropical forests? A 17-year record from Panama. *Ecology, 85*(2),484–489.

Wright, S. J., Yavitt, J. B., Wurzburger, N., Turner, B. L., Tanner, E. V. J., Sayer, E. J., et al. (2011). Potassium, phosphorus, or nitrogen limit root allocation, tree growth, or litter production in a lowland tropical forest. *Ecology, 92*(8), 1616–1625.http://dx.doi.org/10.1890/10-1558.1.

Yorke, S.R., Schnitzer, S.A., Mascaro, J., & Letcher, S. G. (2013). Increasing liana abundance and basal area in a tropical forest: The contribution of long-distance clonal colonization. *Biotropica, 45*(3), 317–324.